TENTH WORLD CONGRESS ON THE THEORY OF MACHINES AND MECHANISMS
Oulu, Finland, June 20 - 24, 1999

SOLVING IMPACT INTERACTIONS USING THE REGULARIZED MODEL APPROACH

Andrés Kecskeméthy, Christian Lange
Institute of Mechanics, University of Technology of Graz
Kopernikusgasse 24, A-8010 Graz, Austria
email: {kecskemethy,lange}@mech.tu-graz.ac.at

keywords: dynamics, multibody systems, impact modeling, regularized model

Abstract

The analysis of collisions in multibody systems has been a topic of continuous research in recent years. Traditionally, impact response is predicted by rigid-body models in conjunction with impact hypotheses, such as Poisson's, Newton's, or Stronge's [1, 2, 7]. An alternative scheme — termed 'regularized model' — is to account for impact interactions through contact elements featuring tangential and normal compliance as well as slip-stick effects. The paper derives analytical solutions for the case of a planar, rough, oblique, eccentric, fully elastic planar impact, showing that large discrepancies may occur between the predicted impact responses of the rigid and regularized models. Finally, an object-oriented multibody generalization and an engineering application are briefly described.

1 Basic Impact Characteristics

Consider the impact of a planar body with a rough horizontal surface featuring coefficient of friction μ (Fig. 1). In order to keep the expositions simple, the body is regarded as a homogeneous bar of length 2ℓ, mass m and radius of gyration ρ, the extension to the two-body planar collision problem being straightforward. The velocity of the bar is given by its angular speed $\dot{\varphi}$ and the velocity $\underline{v} = [\dot{x}, \dot{y}]^{\mathrm{T}}$ of contact point O. Superscripts '$^-$' and '$^+$' denote quantities at the start and end of impact, respectively. During impact, all applied and gyroscopic forces, as well as any change of configuration, is neglected. Relevant external effects are the contact forces $\underline{F}(t) = [F_x(t), F_y(t)]^{\mathrm{T}}$ and the impulses $\underline{P}(t) = [P_x(t), P_y(t)]^{\mathrm{T}} = \int_{t^-}^{t} \underline{F}(\bar{t})\, \mathrm{d}\bar{t}$. As initial conditions, let the bar approach the contact plane with pure translational velocity $\underline{v}^-$ and angle φ with respect to the surface normal. Newton's second law produces two equations of motion which can be expressed in the acceleration of the contact point and the angular acceleration of the bar. This angular acceleration can be back substituted using Euler's equation, yielding two equations of motion which,

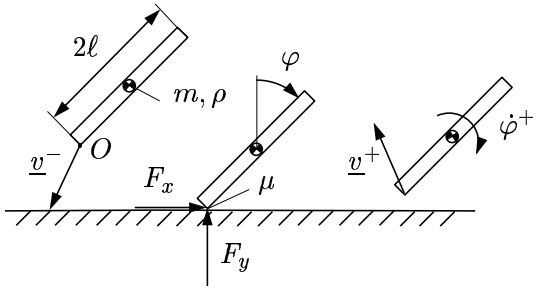

Figure 1: Planar bar on a rough surface

upon setting $\lambda_x = (\ell/\rho)\sin\varphi$, $\lambda_y = (\ell/\rho)\cos\varphi$; $C_{xx} = 1+\lambda_x^2$; $C_{yy} = 1+\lambda_y^2$; $C_{xy} = -\lambda_x\lambda_y$ integrating with respect to time on both sides, yield

$$\begin{bmatrix} \ddot{x} \\ \ddot{y} \end{bmatrix} = \frac{1}{m}\begin{bmatrix} C_{xx} & C_{xy} \\ C_{xy} & C_{yy} \end{bmatrix}\begin{bmatrix} F_x \\ F_y \end{bmatrix} \doteq \frac{1}{m}\,\mathbf{C}\,\underline{F} \quad \Rightarrow \quad \underline{v}^+ = \underline{v}^- + \frac{1}{m}\,\mathbf{C}\,\underline{P}^+ \ . \qquad (1)$$

2 Rigid-Body Model

Using Eq. (1), the impact response can be immediately established once $\underline{P}^+$ is known. A method for approximately determining these quantities, as originally proposed by Routh [5], and further developed in [2, 6, 7], is to track the impulse process in the 'impulse plane' with coordinate axes P_x, P_y until lift-off is established. Hereby, two 'axiomatic' assumptions are made: (I) contact zone deformation occurs in normal direction but not in tangential direction; (II) for impact termination, one of the following hypotheses holds: (1) Newton: $\dot{y}^+ = -e\,\dot{y}^-$; (2) Poisson: $P_y^+ = (1+e)\,P_y^C$; (3) Stronge [6]: $D_R = -e^2\,D_C$, where e is the coefficient of restitution; D_C is the strain energy stored up to the end of compression; D_R is the strain energy released from end of compression until end of impact; and P_y^C is the normal impulse accumulated up to the end of compression. For the elastic case, which is regarded here, $e = 1$. Tracking of impact starts at the origin of the impulse plane in *sliding* mode (assumption I), i.e., along the *'line of sliding'* $P_x/P_y = \pm\mu$ (cf. Fig. 3). This line may intersect the *'line of sticking'* obtained by setting $\dot{x}^+ = 0$ in the first line of Eq. (1), or lead to lift-off before. At the intersection point, the system either switches to stiction, or, if the tangential force is too large, to 'reverse sliding', which is the line passing through the intersection point with the negative slope of the starting line of sliding. Impact terminates when the hypothesis chosen by the user is fulfilled.

3 Regularized Model

When impact velocities are small compared to wave travel velocity in the colliding bodies, the tangential and normal compliances of the impact zone can be modeled by massless springs [3]. With wave travel velocities between 46 m/s (rubber) and 5200 m/s (steel), this is the case for most technical impact problems. Slip-stick effects can be taken into account by introducing a massless 'sledge' which slides for contact forces outside the friction cone. In this model, O represents the contact point, x and y are the deflections of the contact springs, x_S is the location of the center of the sledge (Fig. 2), and $\hat{x} = x_S + x$. This gives rise to two types of governing equations:

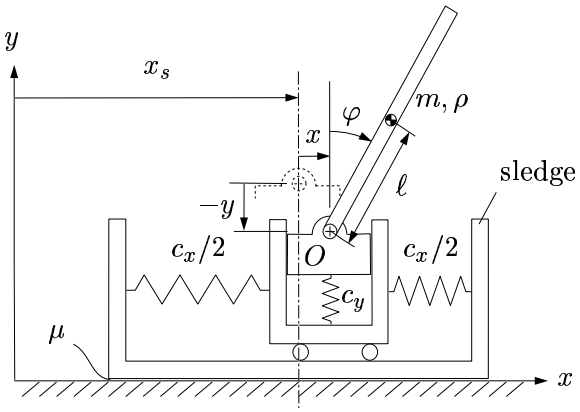

Figure 2: Regularized model

sticking case

$$F_x = -c_x x \ , \ F_y = -c_y y \ , \ \kappa = c_x/c_y$$

$$\begin{bmatrix} x'' \\ y'' \end{bmatrix} + \begin{bmatrix} \kappa\,C_{xx} & -C_{xy} \\ -\kappa\,C_{xy} & C_{yy} \end{bmatrix}\begin{bmatrix} x \\ y \end{bmatrix} = 0 \ ,$$

sliding case

$$F_x = \mu^\star F_y \ , \ F_y = -c_y y \ , \ \mu^\star = \mu\,\mathrm{sign}(\dot{x}_S)$$

$$\begin{bmatrix} \hat{x}'' \\ y'' \end{bmatrix} + \begin{bmatrix} 0 & \mu^\star\,C_{xx} - C_{xy} \\ 0 & C_{yy} - \mu^\star\,C_{xy} \end{bmatrix}\begin{bmatrix} \hat{x} \\ y \end{bmatrix} = 0 \ , \qquad (2)$$

prime denoting differentiation with respect to dimensionless time $\tau = \sqrt{c_y/m}\,t$. Note that the governing equations now only depend on dimensionless parameters. In particular, the stiffness ratio κ may be bounded even for $c_x, c_y \to \infty$, i.e., for high absolute stiffness of the material. Indeed, Routh's assumption $\kappa \to \infty$ is quite unrealistic for technical applications, as e.g. for collision of two spheres of similar material featuring Poisson's ratio $\nu = 0.3$, where it holds $\kappa = 0.824$ [3]. Due to the linearity and time-independency of the governing equations, the latter can be solved in terms of the initial conditions $\underline{x}_0 = \underline{x}(0) = [\,x_0\,,\,y_0\,]^{\mathrm{T}}$, $\underline{x}'_0 = \underline{x}'(0) = [\,x'_0\,,\,y'_0\,]^{\mathrm{T}}$ in each case by simple modal analysis.

3.1 Time History for Sticking Case

For the solution of the equations of motion (2), let $\underline{x}\,(\,\tau\,) = \underline{r}\,e^{i\,\omega\tau}$ where $\underline{r} = [r_x, r_y]^{\mathrm{T}}$ is the eigenvector and ω is the eigenfrequency, i.e., the square root of an eigenvalue

$$\lambda_{1,2} = \frac{1}{2}\left[\kappa\,C_{xx} + C_{yy} \pm \sqrt{(\,\kappa\,C_{xx} - C_{yy}\,)^2 + 4\,\kappa\,C_{xy}^2}\right] \tag{3}$$

Substituting for C_{xx}, C_{yy}, C_{xy}, one first verifies that both eigenvalues are always positive, and hence always *two* real eigenfrequencies exist. With the matrix of eigenvectors

$$R = [\underline{r}_1\,,\underline{r}_2] \quad , \quad \underline{r}_1 = \begin{bmatrix} C_{xy} \\ \kappa\,C_{xx} - \lambda_1 \end{bmatrix} \quad , \quad \underline{r}_2 = \begin{bmatrix} C_{xy} \\ \kappa\,C_{xx} - \lambda_2 \end{bmatrix} \tag{4}$$

the (purely oscillatory) time response for displacements and velocities becomes

$$\underline{x}(\tau) \;=\; R\left[\mathrm{diag}\,\{\,\cos\omega_i\tau\,\}\,R^{-1}\,\underline{x}_0 + \mathrm{diag}\{\frac{\sin\omega_i\tau}{\omega_i}\,\}\,R^{-1}\,\underline{x}'_0\right] \quad , \tag{5}$$

$$\underline{x}'(\tau) \;=\; R\,\left[-\mathrm{diag}\,\{\,\omega_i\,\sin\omega_i\tau\,\}\,R^{-1}\,\underline{x}_0 + \mathrm{diag}\,\{\,\cos\omega_i\tau\,\}\,R^{-1}\,\underline{x}'_0\,\right] \quad . \tag{6}$$

Substituting $\mathrm{d}t = \sqrt{m/c_y}\,\mathrm{d}\tau$ in the time-integral for impulse $\underline{P}$ and assuming $\tau_0 = 0$, one obtains with the previous time history

$$\underline{P}(\tau) \;=\; \underline{P}(\tau_0) + \sqrt{\frac{m}{c_y}}\int_{\tau_0}^{\tau}\underline{F}(\tau)\,\mathrm{d}\tau = \sqrt{\frac{m}{c_y}}\begin{bmatrix} -c_x & 0 \\ 0 & -c_y \end{bmatrix}\int_{\tau_0}^{\tau}\underline{x}(\tau)\,\mathrm{d}\tau$$

$$= \underline{P}(\tau_0) - \sqrt{\frac{m}{c_y}}\,\mathrm{diag}\,\{\,\sqrt{k_i}\,\}\,R\left[\mathrm{diag}\{\frac{\sin\omega_i\tau}{\omega_i}\,\}\,R^{-1}\,\underline{x}_0 + \mathrm{diag}\,\{\,1 - \frac{\cos\omega_i\tau}{\omega_i^2}\,\}\,R^{-1}\,\underline{x}'_0\right] \tag{7}$$

3.2 Time history for sliding case

In case of sliding, the resulting eigenvalues and eigenvectors take the form

$$\begin{aligned} \lambda_1 &= 0 \\ \lambda_2 &= C_{yy} - \mu^\star\,C_{xy} \end{aligned} \quad , \quad \underline{r}_1 = \begin{bmatrix} 1 \\ 0 \end{bmatrix} \quad , \quad \underline{r}_2 = \begin{bmatrix} \mu^\star\,C_{xx} - C_{xy} \\ C_{yy} - \mu^\star\,C_{xy} \end{bmatrix} \quad . \tag{8}$$

clearly involving a rigid-body mode in horizontal direction. Furthermore, depending on the values of λ_x, λ_y and $\mu^\star$, the second eigenvalue can attain a positive, negative or vanishing value, giving rise to three cases (for definition of constants a_i, b_i see Table 1):

Case 1: $\boxed{C_{yy} > \mu^\star\,C_{xy}}$ **.** The second eigenvalue is positive and hence a real eigenfrequency $\omega_2 = \sqrt{\lambda_2}$ exists. The ensuing oscillatory motion is then

$$\underline{x}(\tau) \;=\; (a_1 + b_1\,\tau)\begin{bmatrix} 1 \\ 0 \end{bmatrix} + a_2\,\sin(\omega_2\tau - b_2)\,\underline{r}_2 \quad , \tag{9}$$

Case 2 $\boxed{C_{yy} < \mu^\star\, C_{xy}}$ **.** In this case, the second eigenvalue becomes negative and hence horizontal motion is aperiodic and unstable, yielding

$$\underline{x}(\tau) \;=\; (a_1 + b_1\,\tau)\begin{bmatrix}1\\0\end{bmatrix} + a_2\,\sinh(\nu\tau - b_2)\,\underline{r}_2 \quad , \tag{10}$$

Case 3 $\boxed{C_{yy} < \mu^\star\, C_{xy}}$ **.** This is an exceptional situation, giving rise to a quadruple rigid-body mode. The ensuing motion is

$$\underline{x}(\tau) \;=\; (a_1 + b_1\,\tau)\begin{bmatrix}1\\0\end{bmatrix} + a_2\begin{bmatrix}-[\underline{r}_2]_x\,\tau^2/2\\1\end{bmatrix} + b_2\begin{bmatrix}-[\underline{r}_2]_x\,\tau^3/6\\\tau\end{bmatrix} \quad . \tag{11}$$

where $[\underline{r}_2]_x$ denotes the x-component of the eigenvector $\underline{r}_2$.

With these solutions, the transitions from stiction to sliding ($F_x/F_y = \pm\mu$), from sliding to stiction ($\dot{x}_S = 0$), or from contact to lift-off ($y = 0$) can be easily established either by Newton iteration (for the stiction case, where two harmonics involved) or analytically (for the sliding case, where only one transcendental function occurs). For technical applications, it turns out that only one or two transition events can occur during impact. Hence, by choosing appropriate initial guesses, only few Newton steps are needed, yielding a computationally approach for the present case.

constant	Case 1	Case 2	Case 3
a_1	$x_0 - \dfrac{[\underline{r}_2]_x}{\lambda_2}\,y_0$	$x_0 - \dfrac{[\underline{r}_2]_x}{\lambda_2}\,y_0$	x_0
b_1	$x_0' - \dfrac{[\underline{r}_2]_x}{\lambda_2}\,y_0'$	$x_0' - \dfrac{[\underline{r}_2]_x}{\lambda_2}\,y_0'$	x_0'
a_2	$\dfrac{\sqrt{(y_0')^2 + \lambda_2\,y_0^2}}{\omega_2\,\lambda_2}$	$\dfrac{\sqrt{(y_0')^2 - \lambda_2\,y_0^2}}{\nu\,\lvert\lambda_2\rvert\,\cosh(2b_2)}$	y_0
b_2	$\tan^{-1}\dfrac{-\lambda_2\,y_0}{y_0'}$	$\tanh^{-1}\dfrac{\nu\,y_0}{-y_0'}$	y_0'

Table 1: Integration constants for sliding cases

3.3 Results

Fig. 3 shows the impact responses for $m = 1\,\mathrm{kg}$, $\rho = 1/(2\sqrt{3})\,\mathrm{m}$, $\ell = 0.5\mathrm{m}$, $\varphi = 45°$, $\mu = 1$, $\underline{v}^- = [0.8, -1]^{\mathrm{T}}\mathrm{m/s}$. The two solid lines represent the response of the regularized model for $\kappa = 1$ and $\kappa = 100$, respectively, while the dashed lines are used to construct the impact response for the rigid-body case. Clearly, the regularized model converges to the rigid-body approach for $\kappa \to \infty$.

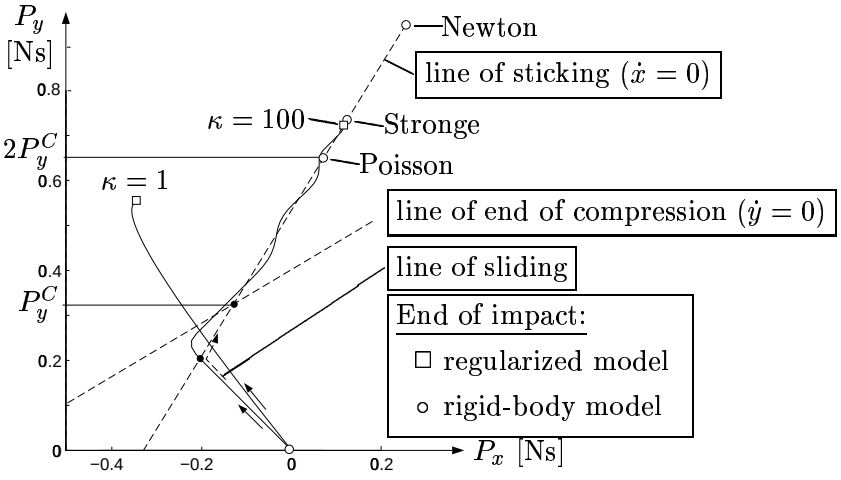

Figure 3: Impact process diagram for planar-bar example

However, only Stronge's hypothesis predicts accurately the impact response, while Newton's and Poisson's hypotheses lead to significant errors, e. g., in the predicted dissipated energy in normal direction as described by D_N (Table 2). Moreover, for the case $\kappa = 1$, the solution of the regularized model is far from that of the rigid-body model; here, the discrepancies are in the range of 40% for angular velocity and even larger for tangential velocity, for which the rigid-body models completely fail to predict a non-zero value. Thus the rigid-body impact assumptions may yield extremely questionable results when the impact is oblique and subject to friction.

	regular. $\kappa = 1$	regular. $\kappa = 100$	Newton	Poisson	Stronge
$\dot{x}^+$ [m/s]	-0.894	-0.005	0.000	0.000	0.000
$\dot{y}^+$ [m/s]	0.906	0.638	1.000	0.520	0.651
$\dot{\varphi}^+$ [rad/s]	3.816	2.590	2.970	2.461	2.600
D_N [Nm]	0.000	0.000	-0.180	0.048	0.000

Table 2: Comparison of impact responses for planar-bar example

4 Object-oriented Implementation

The implementation of the regularized impact model for the planar bar case described above could be readily carried out using Matlab. However, the analytical solutions derived above can not be used for the general case. In order to deal with these, in the current work the object-oriented multibody software MOBILE was extended with a *state event* objects that can be viewed as 'observers' that monitor a set of user defined scalar functions, e.g., the distance between a point and a plane or a force magnitude. These monitored *root functions* are dynamically collected in a vector $\underline{g}$ of functions that depend on the state vector $\underline{q}$, its time-derivatives, $\dot{\underline{q}}$, $\ddot{\underline{q}}$, and the time t. State events can be added ('initialized') as well as activated and deactivated arbitrarily during simulation (Fig. 4). When the root function turns zero, the event 'fires', causing a special user function to be invoked, e.g., one that loads a new model into the dynamical engine. By employing a numerical integrator with root finding option, this 'firing' can be done with high numerical precision. Besides the state events, also time events and timers are introduced to allow the user to set absolute time points or time intervals at which simulation is stopped. With the object-oriented implementation, more complex application can be simulated. A example is the pneumatically-driven mechanism displayed in Fig. 5. The task of the analysis was to optimize the design such as to reduce the contact forces

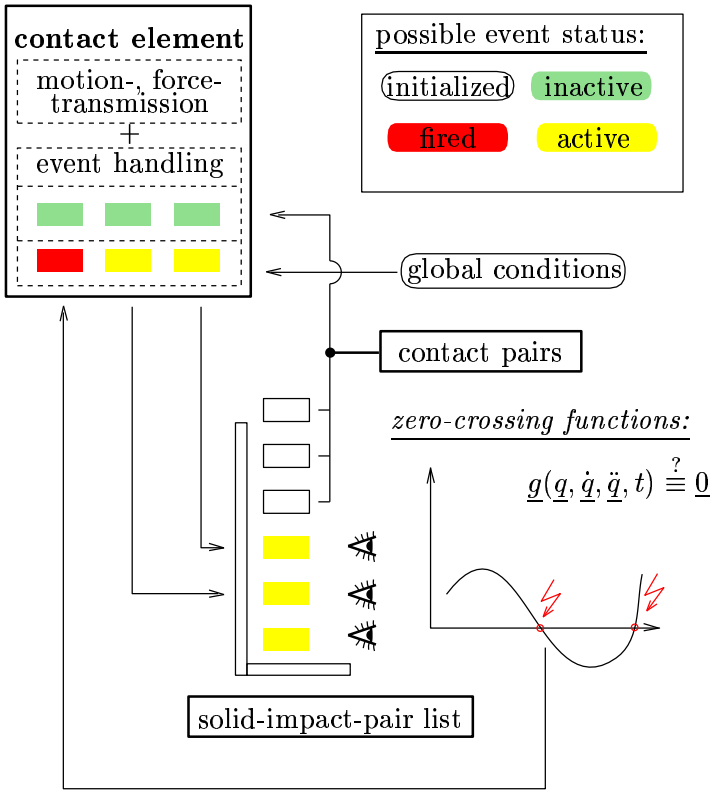

Figure 4: Management of events

that arose when the arms hit the limits (not shown). For the simulation, a total of 10 event handlers where 'attached' to the kinematic skeleton, representing the impact of piston with cylinder heads, contact of arm with environment, and sensors and valves for 'intelligent' control of cylinder chamber pressure. As shown in Fig. 5 (b), after optimization of design and controller, a 30% reduction of contact forces could be achieved.

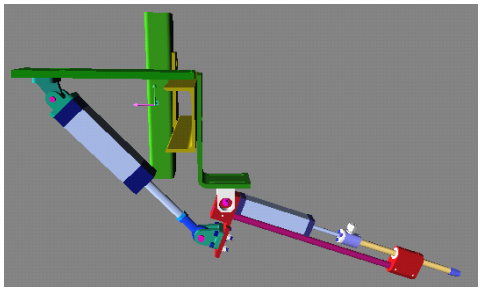

(a) Pneumatically driven mechanism

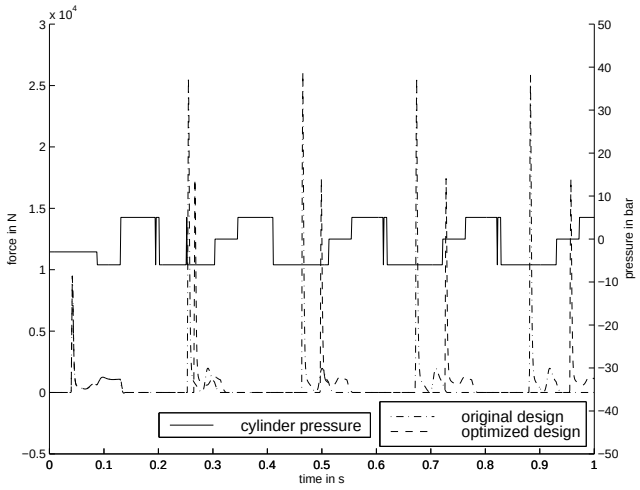

(b) Forces before and after optimization

Figure 5: Example of an engineering application with simple impacts

5 Conclusions

The paper revisits the regularized model for rough, oblique planar impacts, deriving analytical solutions for the sticking and sliding cases. Based on these solutions, an impact of a planar bar with a plane is studied, showing that large discrepancies between the rigid-body impact responses predicted by Newton's, Poisson's as or Stronge's hypothesis and the regularized model can arise. Furthermore, an object-oriented implementation of impacts as well as an engineering application is briefly described.

References

[1] Ch. Glocker and F. Pfeiffer. Dynamical systems with unilateral contacts. *Nonlinear Dynamics*, pages 107–115, 1992.

[2] I. Han and B.J. Gilmore. Multi-body impact motion with friction—analysis, simulation, and experimental validation. *ASME Journal of Mechanical Design*, pages 412–422, 1993.

[3] K.L. Johnson. *Contact Mechanics*. Cambridge University Press, Cambridge, 1985.

[4] A. Kecskeméthy and J. Lüder. Rigid and elastic approaches for the modeling of collisions with friction in multibody systems. *ZAMM*, 1995.

[5] E.J. Routh. *Dynamics of a System of Rigid Bodies*. McMilliam and Co., London, 1991.

[6] W.J. Stronge. Rigid body collisions with friction. *Proc. R. Soc. London*, pages 169–181, 1991.

[7] Y. Wang and M.T. Mason. Two-dimensional rigid-body collisions with friction. *ASME Journal of Applied Mechanics*, pages 635–642, 1992.